THE PHYSICS OF DILUTE 2D ELECTRON AND HOLE SYSTEMS IN SI-BASED HETEROSTRUCTURES

by Marie D'Iorio
Institute for Microstructural Sciences, National Research Council of Canada, Ottawa, Ontario K1A 0R6

INTRODUCTION

Starting with the discovery of the Quantum Hall Effect at the beginning of the 1980's, the field of low dimensionality electron systems has known an incredible expansion. In semiconductors, the confinement of charge carriers in two or fewer dimensions provides added richness from both the fundamental and the applied physics viewpoint. Solid state vocabulary has expanded to include the integer and the fractional Quantum Hall Effects (IQHE, FQHE), skyrmions, composite fermions, high electron mobility transistors (HEMT), modulation doped field effect transistors (MODFETs), resonant tunneling diodes (RTD) etc. In the quantum limit of low temperature and finite magnetic field where the mobility μ and the magnetic field B are such that $\mu B >> 1$, charge carriers confined at the interface between two semiconductors or between a semiconductor and an insulator behave as a gas of non-interacting particles (electron gas), while, in the extreme quantum limit where the cyclotron energy $\hbar\omega_c$ is much larger than the thermal energy k_BT, the fluctuations promote the formation of a liquid state. It was natural then to look for the third state of matter, the solid in two dimensions. This idea was not new, as it had been addressed by Eugene Wigner in 1934 [1] for three dimensional metallic systems. Wigner predicted that, at zero magnetic field, the density of the carriers could be reduced such that the Coulomb exchange would be larger than the thermal disordering energy, thus favoring the crystallization of electrons onto lattice sites. This was later applied to the two-dimensional case where the conditions for observing the electron solid are less stringent than in three dimensions [2,3].

BACKGROUND

There are two regimes for the formation of a solid phase depending on whether the competing fluctuations are thermal or quantum in nature.

(a) In the classical regime, the zero point energy is much smaller than the thermal energy k_BT:

$$k_BT_F = \hbar^2/(m^* a^2) << k_BT$$

where $a = (\pi n_s)^{-1/2}$ is the radius of the Wigner-Seitz cell, n_s is the carrier density, T_F is the Fermi temperature and m^* is the effective mass. The parameter of interest is the ratio between the Coulomb correlation energy and the thermal disordering energy. This is expressed as:

$$\Gamma = V_c/(k_BT)$$

where $V_c \sim e^2/\varepsilon a$ and ε is the dielectric constant.

When Γ is large, the formation of a solid is favored over that of the liquid. Electrons on a helium film provided the first observation of a classical Wigner solid at zero magnetic field and the melting temperature was found to occur at $T_{mc} = V_c/(\Gamma_m k_B)$ with $\Gamma_m = 127 \pm 3$ [4-8].

(b) The quantum regime occurs at low temperatures when $T << T_F$ and the parameter of interest is the ratio of the Wigner-Seitz radius, a to the Bohr radius a_B:

$$r_s = a/a_B = V_c/(k_BT_F)$$

and

$$a_B = \hbar^2\varepsilon/(e^2m^*)$$

The electrons order into a Wigner crystal when r_s is large and the Coulomb correlations dominate; as the carrier density increases and r_s decreases the quantum fluctuations grow until the long range order disappears and the solid melts. This occurs at a critical value $r_s^w = 37 \pm 5$ or critical density $n^w = \pi/(r_s^w a_B)^2$ as determined by a finite size, zero temperature calculation [9].

(c) It is also possible to induce the crystallization of electrons by applying a magnetic field perpendicular to the layer and localizing the electrons within a magnetic length $l_c = (\hbar c/eB)^{1/2}$, smaller than the Wigner-Seitz radius a. The quantum fluctuations are quenched and there is little overlap between the electron wavefunctions. The ratio of the zero point energy to the magnetic or cyclotron energy $\hbar\omega_c$ where $\omega_c = eB/m^*c$ is provided by the filling factor $\nu = 2(l_c/a)^{1/2}$. The magnetically induced Wigner solid is expected to form at finite temperature at a filling factor smaller than some critical value ν_c which has been estimated to be between 1/3 and 1/11. The phase diagram is illustrated in Fig. 1.

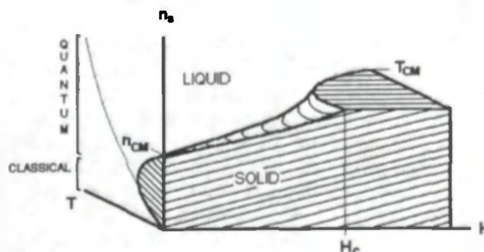

Fig. 1 The phase diagram for the classical and quantum Wigner solid indicating the classical melting temperature, the critical melting density and critical magnetic field.

Experimentally, the problem lies in the fact that the carrier density required for observing the quantum solid phase is very low in III-V semiconductors which typically have low effective masses and large dielectric constants: $r_s \sim 2\text{-}4 << r_s^w$. Electrons on helium have the opposite problem where the density is kept low to avoid a destructive instability of the helium surface: $r_s \geq 10^3 >> r_s^w$. The search should thus focus on material systems with a large effective mass, a low dielectric constant, and in situ density tunability. We should also search for other material features which favor the onset of crystallization. This is the approach that we will be discussing.

What are the signatures for the formation of the Wigner solid phase? Just like its liquid counterpart, the electron solid is a collective phase; this is in contrast to the gas phase where the picture of a non-interacting gas usually suffices. The solid, however, should have rigidity which will distinguish it from a collective liquid state. From magneto-transport experiments, one would expect some extremely large resistance associated with the localization of the charge carriers onto lattice sites and their inability to participate in the transport. But that in itself is not sufficient since single-particle localization will also lead to insulating behavior. The current-voltage characteristics could however provide unambiguous evidence for a solid phase. The presence of an electric field threshold conduction is indicative of rigidity: below threshold, the electrons are pinned which is not possible in a liquid phase, while, above threshold, a collective sliding motion of the depinned electron solid occurs. The resistance below threshold is usually activated due to electrons excited across a "single-electron" disorder induced gap. The conduction here can involve the transport of electrons along the grain boundaries of the Wigner solid or the transport of dislocation pairs. A low value of threshold field implies a long correlation length with respect to the Wigner-Seitz radius. Another signature of the Wigner solid is the increase of broadband noise as the threshold field is approached; this corresponds to the onset of sliding and the noise generated by the electron lattice sliding by the pinning centers. There also should be a temperature above which the thermal disordering energy takes over and the solid "melts" as well as a critical carrier density above which the zero point oscillation energy overtakes the Coulomb interaction [10].

The work on the formation of the classical Wigner crystal using electrons on a thin helium film set the stage for efforts in semiconductors. The substrate under the helium film can provide

sufficient surface roughness to pin the Wigner crystal formed by the electrons. Associated with this pinning are non-linear current-voltage (*I-V*) characteristics which were first observed by Kajita [11]. Above a threshold electric field, the depinned crystal slides like a sliding *charge* density wave. Experiments on a two-dimensional sheet of electrons injected on a helium film (thickness 200-400 A), supported by a glass substrate, have shown that the transport properties of the pinned electron lattice are very similar to that of one-dimensional sliding charge density waves: characteristic non-linear *I-V* curves, melting temperature, and broadband noise generation [12].

The initial effort in identifying a Wigner crystal phase in semiconductors was carried out in GaAs/AlGaAs heterostructures [13-15]. There, it was not possible to decrease the density sufficiently to observe the Wigner crystal at zero magnetic field. Thus the experimental efforts were focused on the magnetic field induced Wigner crystal in the fractional quantum Hall regime. At low fields, the quantum fluctuations dominate the Coulomb correlations and the Integer Quantum Hall Effect (where $\rho_{xy} = h/\nu e^2$ and $\rho_{xx} \rightarrow 0$, ν is an integer) is observed when weak disorder pins the Fermi level in the gap between Landau levels. As the field is increased further, the electrons behave as a correlated quantum liquid which exhibits the Fractional Quantum Hall Effect (where $\rho_{xy} = h/\nu e^2$ and $\nu = p/q$ and p and q are integers and q is odd). A textbook example of these phenomena is shown in Fig. 2. Transitions to an electron solid phase are possible depending on which phase has the lowest ground state energy. Compelling evidence for the magnetic field induced Wigner solid have been provided by electrical, radio-frequency and optical magneto-transport experiments near filling factor 1/5, 2/7 in n-type GaAs/AlGaAs heterostructures and 1/3 in similar p-type samples [16].

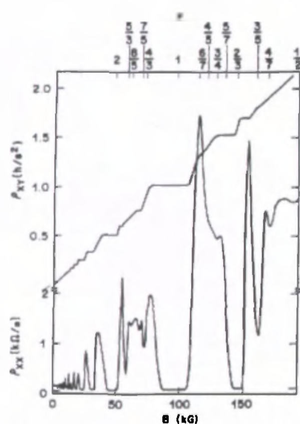

Fig. 2 Textbook example of the Integer and Fractional Quantum Hall Effects. From A. Chang, *The Quantum Hall Effect*, ed. R. E. Prange and S. M. Girvin, Springer-Verlag, New York, 2nd Ed. (1990).

In order to observe a quantum Wigner crystal, in the zero field limit predicted by Wigner, one must look for a material system with large effective mass to minimize the zero point oscillation energy and a small dielectric constant to maximize the Coulomb correlation energy. Moreover, it is important to be able to vary the density in a reliable and reproducible fashion. Almost optimal conditions can be created in several Si-based materials as shown in Table 1.

Table 1. Comparison of parameters of interest for Wigner crystallisation

Parameter	Si / SiGe	Si / SiO$_2$
Electron effective mass : m^*	0.44	0.19
Dielectric constant : $<\kappa>$	12	7.7
Bohr radius : $a_B = \frac{(4\pi\varepsilon_o)(\hbar^2\kappa)}{m^* e^2}$	14 Å	20 Å
Interelectron spacing : $a = \frac{1}{\sqrt{\pi \cdot n_s}}$	126 Å @ $n_s = 2 \times 10^{11}$ cm^{-2}	182 Å @ $n_s = 9.6 \times 10^{10}$ cm^{-2}
Wigner-Seitz radius : $r_s = \frac{a}{a_B}$	9	9
Critical concentration for quantum cold melting : $n_q^{cm} = \frac{1}{\pi \cdot (r_c \cdot a_B)^2}$ where $r_c = 37 \pm 5$	(0.92 - 1.59) x 10^{10} cm^{-2}	(0.43 - 0.70) x 10^{10} cm^{-2}

Other than the physical parameters of the material, it is possible to choose a system which, by its epitaxial layered growth, can enhance the formation of the Wigner crystal. It is known that the coupling between two electron systems separated by less than the interelectron distance favors Wigner crystallization [17-18]. Here, we will look at two systems: Si-SiO$_2$ field effect transistors or Si-MOSFETs (metal oxide semiconductor field effect transistor) and p-type Si-SiGe-Si heterostructures.

SAMPLES

A number of Si-MOSFETs grown in Russia were studied in detail. The electron mobility in these samples is an order of magnitude larger than that of commercial Si-MOSFETs and 2-4 times larger than that of the best Si-MOSFETs grown for research purposes. This mobility was achieved by careful processing to avoid highly diffusive contaminants such as Na and K ions, and repeated growth and stripping of the thermal oxide to ensure a smooth interface. The samples have the following low temperature peak mobilities: Si-15: $\mu = 7.1 \times 10^4$ cm^2/Vs, Si-5: $\mu = 4.3 \times 10^4$ cm^2/Vs, Si-11: $\mu = 3.63 \times 10^4$ cm^2/Vs, and Si-2: $\mu = 2.42 \times 10^4$ cm^2/Vs. By applying a bias to the Al top gate, the carrier density can be varied from 5×10^{10} to 10^{12} cm^{-2}. The longitudinal resistance is measured using a four probe technique with a differential electrometer and DC currents as low as 0.1 pA. The Oxford Instrument low temperature system consists of a top loading 400 μW dilution refrigerator (25 mK < T < 4.2 K) and a superconducting magnet (H = 0-15 Tesla @ 4.2 K). One of the main differences between Si-MOSFETs and GaAs/AlGaAs modulation doped heterojunctions is the location of the dopants which control the scattering events and hence limit the mobility. In Si-MOSFETs the dopants are located in the Si close to the inversion layer. The scattering is short range in this case. In contrast, the III-V heterostructures have dopants separated from the two-dimensional layer by a spacer layer and the scattering is long range. Table 2 shows a comparison of these samples with those used in the study of magnetic field induced Wigner crystal from the point of view of "inherent disorder".

Table 2
Relative Disorder in Very High Mobility Si-MOSFETs and GaAs-AlGaAs Heterostructures

	Si-MOSFETs	GaAs-AlGaAs
n_i (cm^{-2})	1-3×10^{10}	10^{12}
n_i / n_s	0.1-0.3	10-15
setback distance d	50-100 Å	~500 Å
setback/Bohr radius: d/a_B	2.5-5	5

In the dilute limit, where impurity scattering dominates, the Si-MOSFETs and the GaAs/AlGaAs are equivalent systems.

RESULTS

In probing the dilute density regime below 1×10^{11} cm^{-2}, a number of anomalous features were discovered in the magneto-transport measurements at half-filled Landau levels ($\nu = 5/2$, $3/2$).

Some of these are shown in Fig. 3:

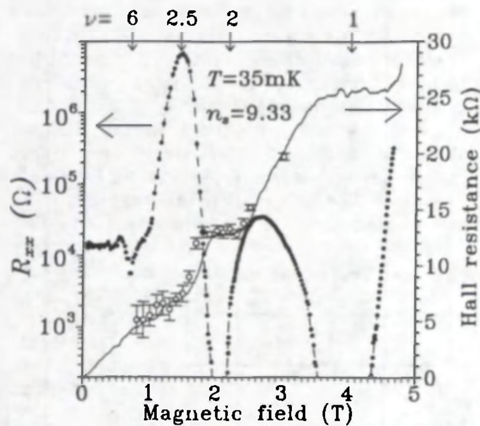

Fig. 3 The longitudinal and Hall resistances as a function of magnetic field for sample Si-5 at carrier density n_s = 9.33 × 10^{10} cm^{-2}.

- Instead of regular Shubnikov-de Haas oscillations obtained from measuring the resistance along the sample as a function of magnetic field, the maxima in the Shubnikov-de Haas oscillation at half-filled Landau levels become enormous with resistances ~ 10^{12} ohms depending on the carrier density. The resistance goes back down to the level of a few ohms as the magnetic field is swept into the quantum Hall minima at filling factors ν = 2 and 1.

- If the magnetic field is kept at one of the SdH oscillation maxima, and the current-voltage (I-V) characteristics are measured at constant density, the result is a sharp non-linear I-V curve with a low threshold field value which increases as the carrier density is decreased:

- The resistance at the SdH maxima is thermally activated below threshold with $\rho_{xx} \propto e^{\Delta/kT}$. The activation energy increases linearly with decreasing density.

- While the large resistance is developing along the sample, the Hall resistance across the sample remains metallic as it does in the high density regime.

These surprising observations [19] led us to believe that the two-dimensional electron gas was undergoing a series of re-entrant transitions from an insulating state characteristic of some new phase to the non-interacting gas of the integer quantum Hall regime. In view of the results attributed to a magnetic field induced Wigner crystal near filling factor 1/5 in GaAs/AlGaAs heterostructures, we looked into the conditions required for Wigner crystallization in Si-MOSFETs and found them to be quite favorable in theory. The large effective mass m^* = 0.19 m_0 and the low dielectric constant ε = 7.7 set Si-MOSFETs apart from GaAs-AlGaAs heterostructures; in addition, Si-MOSFETs feature a two-fold valley degeneracy which is lifted by intervalley interaction and the asymmetric confinement potential (Δ_v = 2.4 K), and a large spin splitting which persists down to zero field (Δ_s = 4 K) due to the large spin-orbit coupling [20].

Because the Fermi energy is comparable to these splittings, polarization effects will be important. While the ground state energetics of the liquid phase is sensitive to the polarization state, the solid phase is relatively unaffected by polarization due to the weaker exchange energy. Whereas the Monte Carlo simulation for a pure system suggests that the transition to the Wigner crystal should occur at r_s = 37 [9], a fixed node and variational Monte Carlo simulation incorporating the valley degeneracy and impurity effects in Si-MOSFETs yield a partially polarized fluid to a fully polarized solid transition at r_s = 7.5 [21]! It should be possible then to observe the quantum Wigner crystal at zero magnetic field in very high mobility Si-MOSFETs!

Theoretically, there is little doubt that, for zero disorder and zero temperature, the 2D electron gas will crystallize into a Wigner lattice upon lowering the density. It is also accepted that, in the limit of strong disorder, single-particle localization will set in. Our samples with minimal disorder provide an intermediate regime where a collective insulating state like the pinned Wigner solid [22] or the pinned charge density wave [23] might exist. The study of the zero field longitudinal resistance as a function of carrier density and temperature led to the following experimental observations:

- Below a critical carrier density n_{sc} ~ 10^{11} cm^{-2}, the longitudinal resistivity exhibits insulating behavior characterized by an exponential rise shown in Fig. 4(a) and a negative slope in the temperature dependence $\partial R_{xx}/\partial T$.

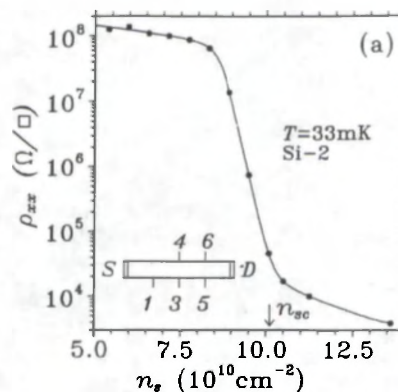

Fig. 4(a) The longitudinal resistivity as a function of carrier density for sample Si-2 at zero magnetic field.

- In the temperature range 100-650 mK, the temperature dependence of R_{xx} can be described by $R_{xx} \propto e^{\Delta/kT}$ where the activation energy Δ drops linearly to zero at n_{sc} as shown in Fig. 4(b).

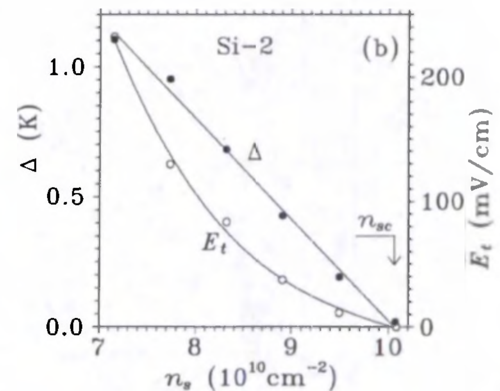

Fig. 4(b) The carrier density dependence of the activation energy and the threshold electric field for sample Si-2. The critical density is n_{sc} = 10.05 × 10^{10} cm^{-2}.

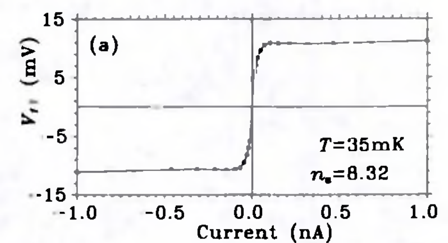

Fig. 5(a) The current-voltage characteristics at carrier density n_s = 8.32 × 10^{10} cm^{-2} and zero magnetic field for sample Si-2.

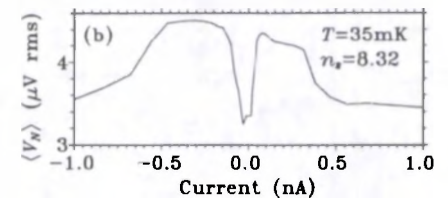

Fig. 5(b) The broadband noise voltage measured between potential contacts as a function of the source-drain current.

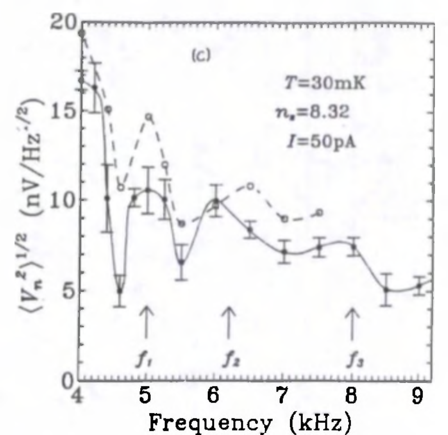

Fig. 5(c) Two independent spectral measurements of the narrowband noise driven by the DC current.

- The current-voltage characteristics exhibit a sharp drop in $\partial V/\partial I$ above a threshold electric field E_t as shown in Fig. 5(a).

- The threshold field goes to zero smoothly at n_{sc} as shown in Fig. 4(b). The data can be fitted well by a power law $E_t \propto \delta n_s^{\gamma}$ where γ = 1.7-1.8 and $\delta n_s = (n_{sc}-n_s)$ (see Fig. 6). More accurate measurements have actually revealed a small discontinuity at n_{sc} pointing to a first order transition [24].

- The dependencies of the activation energy and the threshold field on carrier density is sample independent. However, the critical carrier density is lower for higher mobility (less disordered) samples.

- The sharp rise in conduction is accompanied by a steep increase of the broadband rms-noise voltage $\langle V_N \rangle$ as a function of current (see Fig. 5(b)). The broadband noise was measured at two nearest potential contacts in the 1-300 kHz frequency band.

- The narrowband noise shown in Fig. 5(c) has a reproducible frequency spectrum which shifts to higher frequency as the driving current is increased. The maxima in the signal amplitude occur at frequencies which can be related to the 2D electron lattice constants.

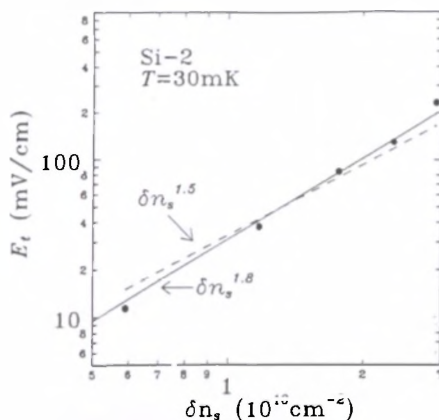

Fig. 6 The dependence of the threshold electric field on the carrier density variation n_{sc}-n_s for sample Si-2. The solid line is a fit to $E_t = \delta n_s^{1.8}$ while the dashed line is the theoretical dependence $E_t = \delta n_s^{1.5}$.

These zero magnetic field transport signatures are similar to those observed in the classical Wigner solid of electrons on helium and the magnetic-field induced Wigner solid near fractional filling factor 1/5. In the very high mobility samples, these features are also seen at filling factors 3/2 and 5/2 at magnetic fields below 5 Tesla. But let us forget this for a moment and play devil's advocate. Could this be simply a manifestation of single-particle localization (SPL)? In disordered semiconductors at low temperature, transport takes place by means of phonon-assisted tunneling to states which are close in energy. The tunneling distance to a state within k_BT of the Fermi energy increases with decreasing temperature. This variable range hopping process has a characteristic power law dependence of the resistivity on the temperature: $\rho(T) = \rho_0 \exp(T_0/T)^x$ where x = 1/3 for single particle localization in 2D without Coulomb interaction [25]. Experimentally, we cannot fit our data to variable range hopping but observe an activated temperature dependence with x = 1; more recent results, in similar samples, have provided evidence for a Coulomb gap (x = 1/2) in the density of states at the Fermi energy, in an intermediate temperature range [26]. In SPL, the threshold conduction is associated with the breakdown of localized states when $eE_t\xi_0$ (where E_t is the threshold and ξ_0 is the localization length) is comparable to the Fermi energy E_F. For the low threshold field at $\delta n_s = 0.1 \times 10^{10}$ cm^{-2} and E_F = 6 K, the localization length would have to be longer than the sample itself i.e. ξ_0 = 6 mm. The threshold field typical of SPL is of order 2.9×10^3 V/cm [27] for our experimental conditions. Our threshold fields are five orders of magnitude smaller. A series of capacitance measurements on these samples also show that the effective area for conduction does not change as the carrier density is decreased [28]. Our experimental results are therefore not consistent with single-particle localization. However, single-particle localization is expected to become dominant in the regime where the number of carriers has been decreased so much that it is equal to the number of pinning impurities in the oxide layer. The more rapid increase of the threshold field below 7.5×10^{10} cm^{-2} is a precursor of this phase.

Let us consider the data in the framework of a pinned Wigner crystal. By drawing an analogy to a charge density wave (CDW), it may be easier to understand the experimental results. Charge density waves are predominantly a one-dimensional phenomenon although they also occur in materials with two or three-dimensional band structures [29]. Chain and layer structures in which CDW transitions have been studied include organic conductors such as TTF-TCNQ (tetracyanoquinodimethane) and linear chain inorganic materials such as TaS_3, $NbSe_3$ and blue bronze $K_{0.3}MoO_3$. In these materials, the electron density is spatially dependent consisting of the unperturbed electron density in the absence of electron-phonon interaction given by $\rho_0 = \pi/k_F$ in one-dimension, and a collective mode formed by electron-hole pairs involving the wave vector $q = 2k_F$:

$$\rho(r) = \rho_0 + \rho_1 \cos(2k_F r + \Phi)$$

where k_F is the Fermi wavevector and Φ is the phase. The collective mode results from the pairing of electron and holes on either side of the Fermi suface to form a condensate called a charge density wave and an accompanying lattice distortion. As in superconductivity, there is a gap in the single-particle excitation spectrum, a collective mode described by a complex order parameter, and a phase whose time and spatial derivatives are linked to electric current and condensate density. Both amplitude and phase fluctuations can occur but whereas the amplitude mode has a gap, the phase excitations are gapless. Pinning is a central concept in CDW physics as the translational symmetry is broken by electrostatic potentials caused by impurities and grain boundaries which serve to pin the collective mode. The CDW systems are composed of normal electrons coexisting with a condensate and scattering with the normal electrons reduce the coherence length. Among the transport properties associated with the dynamics of the collective mode are (1) non-linear electrical conduction with a threshold electric field, (2) a metal-insulator or a metal-semiconductor transition below a distinct melting temperature accompanied by a periodic lattice distortion incommensurate with the underlying lattice, (3) anomalous microwave conductivity, (4) dc and ac excitations dominated by the collective mode dynamics, and (5) strong frequency dependent response in a broad frequency range. In studying such systems it is essential to examine intrinsic defects due to thermal fluctuations as well as defects, vacancies and dislocations induced by quantum fluctuations as they are believed to play an important role in the melting transition.

What drives the conduction in the CDW? Let us imagine that a CDW is pinned by the electrostatic potential well of an impurity . If an external electric field is applied, the CDW deforms around the pinning center but electrons remain constrained by the phase coherent CDW. The electrons which have not condensed in a CDW can still contribute to conduction by thermal activation across the gap but because of their low density the resistivity of the pinned CDW is high. At low temperatures when all electrons have frozen out, the activation energy is related to the energy required to change the phase of the local CDW in a coherent domain by 2π. Above a critical threshold field, the entire CDW can become depinned and slide coherently in the direction opposite to that of the applied electric field. The differential resistivity drops sharply giving rise to sharp non-linear I-V characteristics. The larger the number of pinning impurities, the greater the loss of phase coherence and the smoother the I-V characteristics. As the CDW slides past stationary impurity potentials, the voltage noise generated by the perturbation of the impurity potential will depend on the current, the carrier density and the period of the CDW. The size of the phase coherent domains is defined by the correlation length which can be measured from the transverse shear modulus, the threshold field, the interelectron spacing, and the carrier density.

In analogy to CDW systems, the electron solid forms in the presence of a neutralizing background charge which fixes the density when the potential energy between the localized electrons dominates all other energies in the problem. In most samples, the solid phase coexists with uncrystallized electrons. However, the phase coherence length remains large compared to the interelectron spacing in the electron solid (in GaAs: 4.8 $\mu m >> 100 r_s \sim 300$ Å). Thus quantum depinning and defect waves or dislocation pairs are possible in electron systems but unlikely in CDW. The type of pinning, weak or strong, will depend on the location, nature (acceptor or donor), and number of pinning impurities. A successful model for the conduction mechanism in the Wigner solid has been developed by Chui. The model assumes that the charge carrying excitations are bound dislocation pairs. A single dislocation can be visualized as a shift of the electrons from equilibrium position which can be described by a displacement field. A dislocation pair consists of two dislocations with displacement fields in opposite directions; there is a net displacement of charge between the dislocations and the motion of this locally altered density is possible with resulting conduction. This is equivalent to the phase slip model in CDW.

If we review the experimental results, the similarities between the pinned charge density wave and the pinned electron solid are striking. There is a critical density and a critical temperature below which the insulating phase appears. The transition at the critical carrier density is weakly first order in character. The non-linear I-V characteristics can be interpreted as showing that at small currents the Wigner crystal is pinned by the neighboring impurities until the threshold field is exceeded and the Wigner crystal slides. Over the range of densities 7.2×10^{10} - 1.0×10^{11} cm^{-2} the threshold field decreases as $E_t \propto (n_c - n_s)^{\beta}$ where $\beta = 1.7$-1.8. This is in agreement with a depinning mechanism involving the creation and separation of dislocation pairs [30]. The theoretical model agrees well with the experimental results as shown in Fig. 6. The fact that the sub-threshold activation energy below 100 mK is much smaller than that above is consistent with extended defect conduction [31]. If one ignores quantum coherence effects, the motion of extended defects and in particular that of dislocation pairs is equivalent to phase slippage in a charge density wave [32]. The σ_{xx} versus electric field curves can be fitted to a phase slippage equation of the type:

$$\sigma_{xx} = (I_0/l_c E)e^{(-\Delta/kT)} \sinh[neE l_x/kT]$$

where l_c is the intercontact distance, I_0 is related to the current created by a single phase slip and l_x is a characteristic phase slip length. The value of l_x obtained from the fit in Fig. 7 is 0.23 μm, or ten times the interelectron spacing.

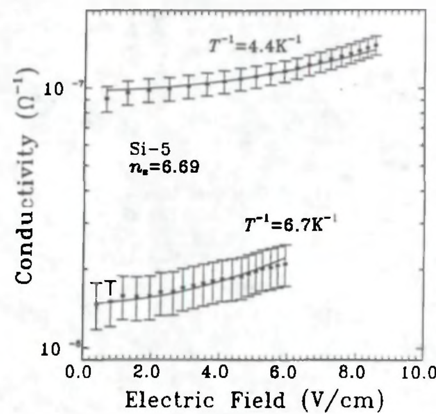

Fig. 7 Conductivity versus applied electric field for sample Si-5 at $n_s = 6.69\times10^{10}$ cm^{-2}. The solid lines are a single fit to the data at both temperatures using phase slip model.

What information can we get about the collective transport of depinned domains above the threshold field? By using the approach of elastic theory [33] as applied to charge density waves in the weak pinning limit, we can estimate the correlation length or domain size, L_D as $(K_T a/(2\pi e n_s E_t))^{1/2}$ where K_T is the transverse shear modulus, and a is the interelectron spacing. The experimental dependence of the threshold field on the carrier density shows that the correlation length diverges as $(\delta n_s)^{0.9}$ and thus L_D becomes smaller as the density is decreased, driving the system towards single-particle localization. Single-particle localization does have "its place in the sun" in the phase diagram.

The activation energy and the threshold field can be used to extract some characteristic length scale for the electron solid, e.g. the elementary crystallite size of the pinned Wigner solid. For a carrier density $n_s = 8.4\times10^{10}$ cm^{-2}, the sample typically consists of pinned crystallites approximately 0.7 μm $\times$ 0.7 μm in size each containing about 300 electrons with an interelectron distance ~ 400 Å!

The generated broadband noise shown in Fig. 5(b) is also consistent with depinning of the Wigner crystal or coherent defect motion above threshold. The narrowband noise should yield frequency peaks related to the principal lattice spacings. If we assume that the electron lattice extends across the entire 2D layer of width w and that the total current I is only provided by the sliding lattice, the spectral maxima will be related to the principal lattice spacing η_i as $\eta_i = I/(e n_s w \eta_i)$. For a hexagonal lattice sliding in a random field of point defects, η_1 = b, $\eta_2 = \sqrt{3}$ b, and η_3 = 2b where b is the distance between nearest neighbor electrons. Experimentalists have been urged to try this extremely difficult measurement as it could provide the definitive signature for lattice ordering of electrons- the "smoking gun" for Wigner crystallization. Although there are peaks in the narrowband spectrum and the frequency shifts with current, there is no simple relation that can be applied to link the results to a hexagonal or triangular lattice symmetry. It is likely that part of the current is provided by "uncondensed" electrons hopping beyond the lattice.

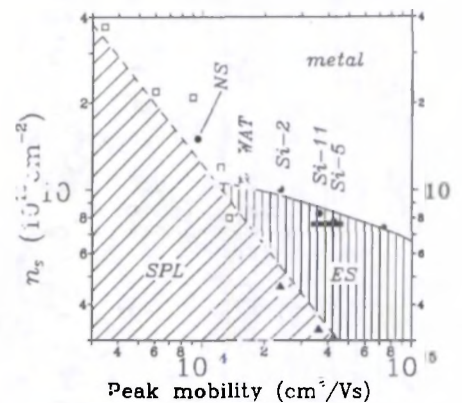

Fig. 8 Phase diagram for the two-dimensional electron system showing the critical density versus the sample peak mobility.

By studying samples in a wide range of mobilities and carrier densities, we have been able to probe the effect of "disorder" on the development of the insulating phase. Fig. 8 shows the phase diagram for the formation of the collective insulator phase or quantum Wigner solid confined between the metallic state above the cold melting boundary n_{cm} (full line) and the Anderson insulator or the regime of single-particle localization below the n_{spl} boundary. By using a calculation by Gold [34] for the mobility of Si(100) inversion layers, we obtain a satisfactory model for the peak mobility versus carrier density in our samples. The number of impurities n_i is a better indicator of disorder as the impurities are the main source of scattering at low densities (below 2×10^{11} cm^{-2}). The boundary for SPL is estimated from n_i and depicted by a short dashed line. This is the highest estimate for SPL in our samples where the surface roughness is much lower than that used to calculate n_i and n_{SPL}. The full triangles indicate n_{SPL} estimates if the domain length L_D is twice the interelectron distance $L_D = 2a$. The solid line is the calculated dependence of the cold melting density on n_i using the mean square displacement as a function of n_i and an estimate of the cold melting density as n_i goes to zero. The calculation of the transition from a polarized WS to a partially polarized liquid at $r_s \approx 10$ ($n_s \sim 7.65\times10^{10}$ cm^{-2}) is represented by a bar [21] and is in agreement with the data for Si-5 and Si-11. This phase diagram also explains why such a collective phase was not observed by other groups using lower mobility samples and suggests that we should be looking for a material system with as good if not better material parameters than the high mobility Si-MOSFETs studied here. Thus there is mounting experimental evidence for a low temperature transition to a collective

insulator at zero magnetic field in high mobility Si-MOSFETs. This collective insulating phase has the transport characteristics of a Wigner solid.

The temperature dependence of the zero field resistance as a function of carrier density is also host to some more fundamental physics: that of scaling and universality. For more than two decades, it has been generally accepted that, at zero magnetic field, all states are localized in a two-dimensional system for an infinite sample as $T \to 0$ [35]. In contrast, a three-dimensional system can sustain a metal-insulator transition because the electrons are localized only when the Fermi energy lies below a mobility edge E_c. The conventional wisdom in 2D systems has recently been questioned as a result of a number of experimental results in superconducting thin films, and in high-mobility Si-MOSFETs [36-37]. In addition, a theoretical study of noninteracting 2D electrons in a model disorder potential with a random set of special scatterers showed that, at zero magnetic field, the system is localized only when $E_F < E_c$ [38]. In material systems where the range of the scattering centers is short (as in MOSFETs), similar to Azbel's model potential, a "true" zero magnetic field metal-insulator transition may be allowed in the limit of zero temperature. The resistivity as a function of temperature over a wide range of densities ($7.12 \to 13.7 \times 10^{10}$ cm^{-2}) in a high-mobility Si-MOSFET sample (Si-12b; μ_{max} = 3.0×10^4 cm^2/Vs) can be made to overlap by scaling along the temperature axis. The resistivity can be represented in terms of a ratio T/T_0 where T_0 depends only on the density. The data collapses on two separate curves one for the insulating side of the transition and the other for the metallic side as shown in Fig. 9. One of the signatures of a phase transition is the scaling of an appropriate physical parameter. It would seem then that the results are in agreement with Azbel's model but in contradiction with that of Abrahams and co-workers; this suggests that there is a "true" metal insulator transition in the two-dimensional electron system in Si at zero magnetic field.

Si-SiGe-Si QUANTUM WELL STRUCTURES

The experimental results on high mobility Si-MOSFETS have been reproduced in at least four different laboratories around the world. However, there is only one batch of such samples and it is very difficult, without a large investment in time and manpower, to fabricate more of these. We have thus turned to pseudomorphic Si-SiGe-Si heterostructures which are grown, either by molecular beam epitaxy or ultra-high vacuum chemical vapor deposition techniques, in a large number of laboratories and may be better suited for studying Wigner crystallization. The important features of the p-type Si-SiGe-Si quantum wells are that the 2D holes have a large effective hole mass, 0.42 m_e which is twice that of electrons in the Si-MOSFETs. This has been checked in our samples by analysis of the low-field Shubnikov-de Haas oscillations and by cyclotron resonance [39-41]. Although the dielectric constant $\varepsilon \sim 12.6$ is similar to that of GaAs-AlGaAs heterostructures, the symmetric confinement of holes in the SiGe well can lead to coupled 2D hole gases. As pointed out in Table 1, at a carrier density of 2×10^{11} cm^{-2} in Si-SiGe heterostructures, the Wigner-Seitz radius is identical to that in Si-SiO_2 and the quantum cold melting critical density is twice as large because of the larger effective mass!

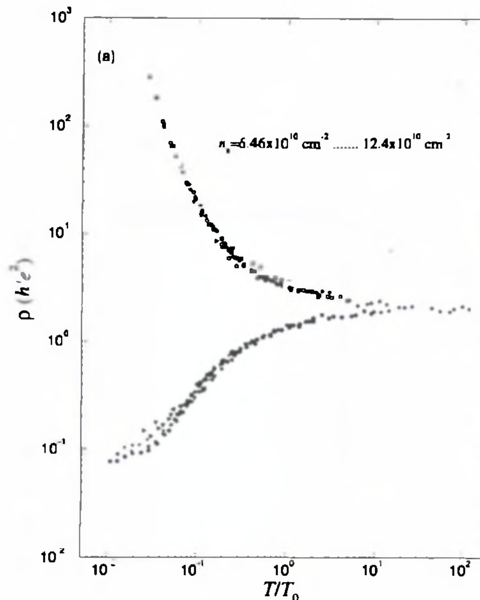

Fig. 9 Resistivity versus T/T_0 where T_0 is the scaling parameter. The open symbols correspond to the insulating side of the transition while the closed ones correspond to the metallic phase.

The $Si\text{-}Si_{0.87}Ge_{0.13}\text{-}Si$ heterostructures were grown on an n Si (100) substrate by molecular beam epitaxy. The symmetrically-doped samples were grown on a 500 Å i-Si buffer and consisted of a 500 Å Si layer modulation-doped with boron acceptors at 10^{18} cm^{-3} and a 300 Å i-Si setback on each side of a $Si_{0.87}$ $Ge_{0.13}$ quantum well of thickness *d*. A set of samples was grown with *d* = 45, 65, 90 and 115 Å. The cap layer consisted of 400 Å of B-doped Si. This is shown in Table 3.

The samples were patterned as Hall bar structures 10 mm long and 2 mm wide. Ohmic contacts were made using Al evaporation and annealing below the eutectic point.

A number of unexpected results were obtained in these samples:

- The SdH oscillations in the 115 Å well are typical of two subband population as shown in Fig. 10. These are not oscillations from two independent hole gases at each interface as was observed in larger wells but rather the population of the heavy hole and the light hole ground subbands. This interpretation is borne out by k•p Luttinger Hamiltonian calculations [41].

Table 3
The MBE-grown $Si\text{-}Si_{0.87}Ge_{0.13}\text{-}Si$ Heterostructures

Surface	
B - doped Si - 1x10^{18} cm^{-3} 900 Å	
i - Si spacer 300 Å	
$Si_{0.87}Ge_{0.13}$	
Sample #	d
SiGe 1456	115 Å
SiGe 1457	90 Å
SiGe 1458	65 Å
SiGe 1459	45 Å
i - Si spacer 300 Å	
B - doped Si - 1x10^{18} cm^{-3} 500 Å	
i - Si buffer 500 Å	
Si (100) n	

- There is a large peak in the longitudinal resistance at filling factor 3/2 followed by a deep minimum at filling factor $\nu = 1$. The Hall resistance is not anomalous at the half-filled Landau level and displays a well developed plateau h/e^2 when the longitudinal resistance is at its minimum.
- For the narrower 90 and 65 Å wells, there are large longitudinal resistance peaks at both ν = 3/2 and 5/2, re-entrant with deep minima at ν = 1 and 2.
- The temperature dependence of the current-voltage characteristics taken at ν = 3/2 for the 65 Å well reveal that the onset of the large resistance maxima (>> h/e^2) occurs around 500 mK (see Fig. 11).

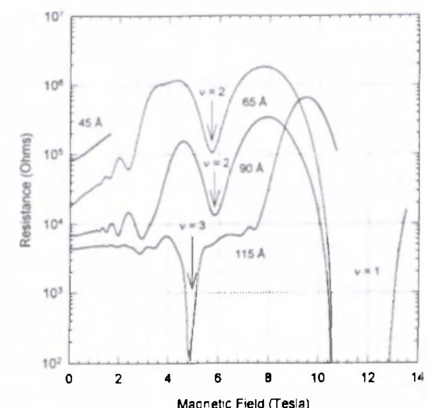

Fig. 10 Longitudinal resistance as a function of magnetic field for different SiGe quantum well widths at T ≈ 25 mK.

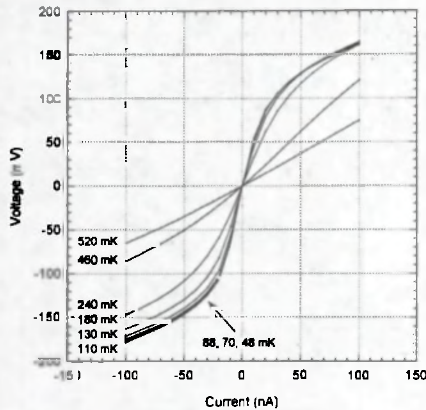

Fig. 11 Current voltage (I-V) characteristics as a function of temperature for ν = 3/2 at B = 7.75 T for the 65 A well.

- Similar results are shown in Fig. 12 for the 90 Å well with the sub-threshold resistance at ν = 3/2 increasing by two orders of magnitude below 500 mK. the inset shows the thermal activation of the differential resistance where $dV/dI \propto e^{-\Delta/kT}$ with Δ = 0.47 K in the temperature range above 100 mK.

Although these results have been taken at a fixed density ~ 2×10^{11} cm^{2}, the basic features of large longitudinal resistances at half-filled Landau levels, non-linear I-V characteristics with low threshold fields, and thermal activation of the resistance are very similar in nature to those in the Si-MOSFETS. In the light of the scaling behavior of the zero magnetic field resistance in Si-MOSFETs, we have also looked at the temperature dependence of the longitudinal resistance at zero field for different well widths.

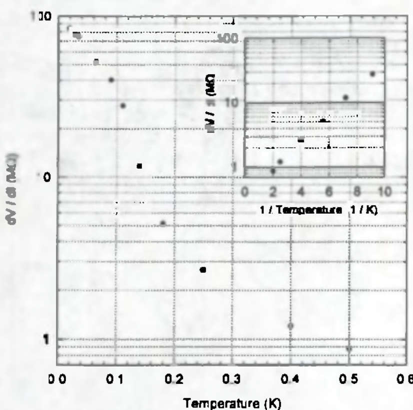

Fig. 12 Temperature dependence of the differential resistance for the 90 A well at ν = 3/2 and B = 7.95 T. The inset shows activated behavior in the higher temperature scale.

As shown in Fig. 13, there is a transition from an insulating phase where ρ_{xx} decreases with temperature for the 65 Å well to a metallic phase where ρ_{xx} decreases with temperature for the 90 Å and 115 Å wells. This is consistent with the fact that the carrier density is decreasing with decreasing well width.

The curves also appear to converge near a critical resistivity of $h/2e^2$. These features are similar to those observed in superconducting thin films of Bi as a function of thickness, and Si MOSFETs and GaAs-AlGaAs heterostructures as a function of carrier density. Further study of scaling parameters will require the variation of the density in the Si-SiGe-Si heterostructures. From other work [42], we know that the critical density in these systems is slightly above our fixed density. We must also investigate the role of disorder in the onset of these transitions by studying higher mobility and hence higher Ge content samples.

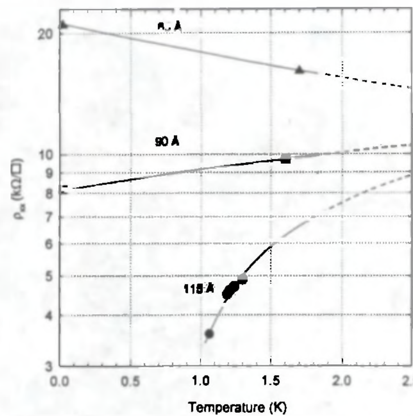

Fig. 13 Temperature dependence of the longitudinal resistivity in a vanishing magnetic field for different SiGe quantum well widths.

CONCLUSION

The work on Si-MOSFETs has provided a phase diagram for the formation of a quantum Wigner crystal at zero magnetic field as a function of disorder. It was also established that a fully spin-polarized Wigner crystal could exist re-entrantly with a partially polarized quantum liquid or gas in the quantum Hall effect regime in very high mobility samples only. The study of the re-entrant insulating phase in semiconductor heterostructures has also led to the definition of a new type of insulator, "the Hall insulator" [43], for which the Hall resistivity remains metallic while the longitudinal resistivity becomes infinite. The system par excellence to study the Wigner crystal state is one where the effective mass is large, the dielectric constant and the amount of disorder are small, the carrier density is tunable and the material system imposes some sort of inherent coupling either with non-degenerate valleys as in Si-MOSFETs, or by lifting the degeneracy between the symmetric and anti-symmetric states through the valence band anisotropy as in the Si-SiGe system. Finally, there is now mounting experimental evidence that the Abrahams-Anderson-Licciardello-Ramakrishnan theory for which a metal-insulator transition in an infinite 2D system, at zero magnetic field as T→0 is forbidden, is inappropriate in 2D systems with short range scatterers.

We have only begun to explore the phase diagram for the formation of a Wigner solid in two-dimensional electron and hole systems. The mapping of the phase boundaries as a function of temperature, density, magnetic field and disorder is a challenging task. As better samples become available, a fuller story on the richness of the dilute density regime can be written.

ACKNOWLEDGMENTS

I wish to acknowledge fruitful collaboration with a number of colleagues: from NRC- Don Brown, John Campbell, Simon Deblois, Pawel Hawrylak, Jennifer Lam, J.-P. Noël, and Duncan Stewart, from the University of Oklahoma- John Furneaux and Sergey Kravchenko, from SUNY in Buffalo- Bruce McCombe and his group and, finally, from the Institute for High Temperature Physics in Moscow- Vladimir Pudalov who provided the Si-MOSFETs and was the driving force behind that work.

REFERENCES

1. E. Wigner, Phys. Rev. 46, 1002 (1934).
2. R.S. Crandall and R.W. Williams, Phys. Lett. A 34, 404 (1971).
3. A.V. Chaplik, Sov.Phys. JETP 35, 395 (1972).
4. A.S. Rybalko, B.N. Esselson, and Y.Z. Kovdrya, Sov. J. Low Temp. Phys. 5, 450 (1979).
5. C.C. Grimes and G. Adams, Phys. Rev. Lett. 42, 795 (1979).
6. R. Mehrottra, B.M. Guenin, and A.J. Dahm, Phys. Rev. Lett. 48, 641 (1982).
7. F. Gallet, G. Deville, A. Valdes, and F.I.B. Williams, Phys. Rev. Lett. 53, 588 (1984).
8. G. Deville, J. Low Temp. Phys. 72, 135 (1988).
9. D. Ceperley, Phys. Rev. B 18, 3126 (1978); B. Tanatar and D. Ceperley, Phys. Rev. B 39, 5005 (1989).
10. For a review see *Physics of the Electron Solid*, edited by S.T. Chui, International Press Inc. Boston (1994).
11. K. Kajita, Jpn. J. Appl. Phys. 25, 1943 (1987); Surf. Sci. 196, 29 (1988).
12. H.-W. Jiang and A.J. Dahm, Phys. Rev. Lett. 62, 1396 (1989); Surf. Sci. 229, 352 (1990).
13. E.Y. Andrei, G. Deville, D.C. Glattli, F.I.B. Williams, E. Paris, and B. Etienne, Phys. Rev. Lett. 60, 2765 (1988).

(continued on page 71)